Letter

Defect-populated configurations in nematic solid tori and cylinders

Javier Rojo-González,[1,2] Livio Nicola Carenza,[3,4] Alexis de la Cotte,[1] Ludwig A. Hoffmann,[3] Luca Giomi,[3] and Alberto Fernandez-Nieves[1,2,5]

[1]*Department of Condensed Matter Physics, University of Barcelona, 08028 Barcelona, Spain*
[2]*Institute of Complex Systems (UBICS), University of Barcelona, 08028 Barcelona, Spain*
[3]*Instituut-Lorentz, Universiteit Leiden, P.O. Box 9506, 2300 RA Leiden, The Netherlands*
[4]*Department of Physics, Koç University, Rumelifeneri Yolu 34450, Sariyer, Istanbul, Turkey*
[5]*ICREA-Institució Catalana de Recerca i Estudis Avancats, 08010 Barcelona, Spain*

(Received 19 June 2023; accepted 1 February 2024; published 27 March 2024)

We make toroidal droplets of nematic liquid crystal and explore the defect-populated stable configurations that appear after heating to the isotropic phase and cooling back to the nematic phase. These configurations, as confirmed by simulations, are made of defect pairs where the positive/negative defect is located in the region of maximum positive/negative Gaussian curvature. Moreover, we demonstrate through experiments and simulations that these defect pairs also appear and are stable in cylinders, which have zero Gaussian curvature, highlighting the crucial role of bulk nematic elasticity in stabilizing these structures.

DOI: 10.1103/PhysRevResearch.6.L012065

Topological defects are common features in condensed matter, affecting the stability and self-organization of complex fluids [1–4]. Defect manipulation in passive liquid crystals, in particular, has been widely studied to promote self-assembly [5–12]. More recently, the coupling between defects, geometry and topology has been pointed to affect and even control processes like tissue morphogenesis [13–15].

In nematics, the number and type of topological defects can be controlled using confinement geometry and surface anchoring [16–28]. For nematic tori with tangential anchoring, the Poincaré-Hopf index theorem establishes that the total topological charge must be zero on the surface [29,30]. This applies to cases without defects, expected for nematics on slender tori, and defect-populated states with equal number of positive and negative defects, which are predicted for nematics on tori with sufficiently small aspect ratio, $\xi = R/a$, with R and a the central-circle and tube radii, respectively [22,27,31]. The appearance of defects on a torus is also accompanied with the coupling between their winding number or topological charge, s, and the Gaussian curvature, K, of the underlying surface, driving defects towards regions of like-signed curvature [31–34]. Experiments to date with nematic solid tori, where the nematic fills the three-dimensional space formed by sweeping a disk around a circle, however, only report the existence of defect-free configurations, with a doubly twisted director field that breaks reflection symmetry and that results from important saddle-splay contributions to the elastic free energy [22].

In this Letter, we subject nematic solid tori to heating and cooling cycles, and find that they most commonly relax to configurations populated with defects. We mainly observe pairs of negative and positive defects, which display the expected coupling with the underlying Gaussian curvature. Remarkably, we also find these defect pairs in nematic solid cylinders, where the inside/outside asymmetry driving the unbinding of the defect pairs on the torus is completely absent. We rationalize our results with lattice Boltzmann computer simulations of the Landau-de Gennes theory for nematic liquid crystals and analytical considerations that unequivocally show that the free energy difference between defect-free and defect-populated states is small, hence making them both equally accessible after the heating/cooling cycles. The nematic rearrangement in the bulk of the torus required to transition between these states introduces a free energy barrier that effectively stabilizes the defect-populated states. By contrast, rearrangements that do not require such bulk reorganization spontaneously occur due to the lack of a free energy barrier.

We generate stable nematic toroidal droplets by injecting 4-cyano-4'-pentylbiphenyl (5CB) through a tip placed off-axis in a rotating cuvette filled with a yield stress material [35–37]. Shear forces induce the formation of a jet that closes onto itself to result in toroidal droplets that are stabilized by the elasticity of the yield stress material [36], which contains polivinyl alcohol (PVA) to ensure parallel anchoring of the nematic director at the surface of the toroids. Using this technique, we generate a first torus with radius $R \sim 520$ μm and tube radius $a \sim 170$ μm, as shown in Fig. 1(a), and an aspect ratio $\xi = \frac{R}{a} \approx 3$. After generating the torus, the nematic relaxes into a stable doubly twisted configuration, similar to the one described in prior work [22], with a twist angle of $\sim 30^\circ$ [37].

Surprisingly, after heating the nematic to the isotropic phase, and cooling it back to the nematic phase, we find that it rarely relaxes to its original defect-free configuration. Most of the time, the relaxed nematic possesses localized features like the one highlighted with a dashed circle in Fig. 1(b).

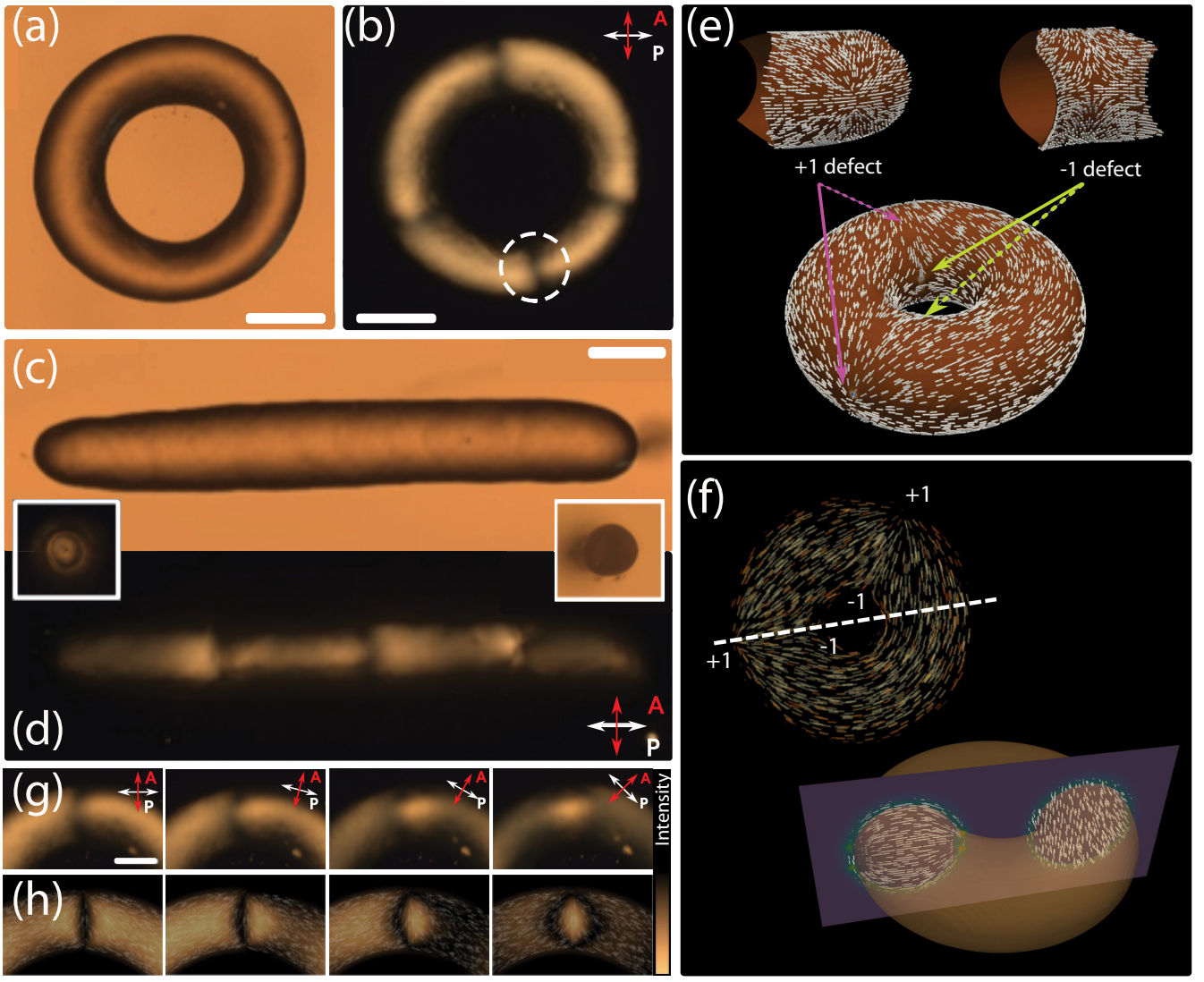

FIG. 1. (a) Bright field top view of an experimental thick torus. (b) Crossed polarizer top view of the thick torus in (a) after heating the nematic to the isotropic phase and cooling back to the nematic phase. Scale bar: 400 μm. (c,d) Bright field and crossed polarizers top view of an experimental cylinder. The inset corresponds to the side view of the cylinder. Scale bar: 400 μm. (e) Snapshot of the simulated torus including the nematic director field on its surface (white lines). In this configuration, we find two integer defect pairs with the positive/negative defects located on the region of maximal positive/negative curvature. At the top, we show a closeup of the nematic field on the surface in the vicinity of a $+1$ and a -1 defect. (f) Top: horizontal cross section of the same torus where defects are located on the left, but not on the right side. Bottom: vertical cross section of the torus showing the nematic director field inside the torus. (g) Experimental textures when rotating the crossed polarizers. Scale bar: 200 μm. (h) Simulation textures of nematic configurations associated to the expected experimental director field organization.

Importantly, these features are stable, and their number and location change after each thermal cycle [37]. Furthermore, they are void of any disclination lines.

We hypothesize they are pairs of $+1$ and -1 point defects, located on the surface near the outer and inner rings of the torus; this explains why we do not see them in our top views of the nematic toroid, and why the presence of a single pair, which we occasionally observe, does not violate the Poincaré-Hopf index theorem. Note that since the nematic fills the full volume of the torus, we expect the defects, if present, to have full integer topological charge, in contrast to the half-integer defects observed for nematics confined to the toroidal surface [27,38].

To test our hypothesis, we perform lattice Boltzmann simulations where we confine the liquid crystal to a toroidal droplet and enforce tangential anchoring at the boundary. The dynamics of the system is ruled by the Landau-de Gennes theory for nematic liquid crystals, and the equations of motion are integrated using a hybrid lattice Boltzmann approach [37,39,40]. The nematic field is relaxed from a high temperature configuration, analog to the isotropic phase, until a steady-state configuration is reached. The simulations show that ± 1 pairs of defects are indeed stabilized, with the positive/negative defect located in the outer/inner ring of the torus, as shown in Figs. 1(e) and 1(f), and consistent with our experimental findings and other Monte Carlo simulations [41]. To further

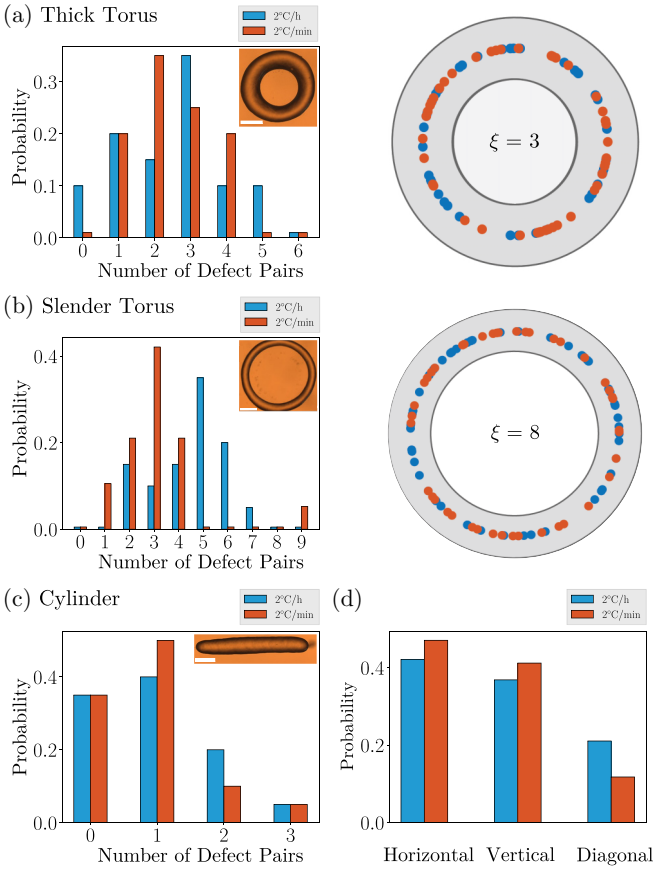

FIG. 2. (a) Left: histogram of the number of defect pairs in a thick nematic torus with $\xi \approx 3$ for two different cooling rates. Right: azimuthal distribution of the location of the defect pairs. (b) Left: histogram of the number of defect pairs in a slender nematic torus with $\xi \approx 8$. Right: azimuthal distribution of the location of defect pairs. (c) Histogram for the number of defect pairs for a cylindrical nematic. (d) Histogram associated to the location of defect pairs for a cylindrical nematic. Scale bar in all bright field images: 400 μm.

corroborate the hypothesis that this defect structure is the one observed in our experiments, we compare experimental polarized optical microscopy (POM) images with those obtained from simulations. We do so by rotating the crossed polarizers and observing the resulting change in texture. The good agreement between experiments and simulations, shown in Figs. 1(g) and 1(h), confirms that the features seen in nematic solid tori are indeed due to ±1 defect pairs. Note that the defect pair structure, with a positive defect located in the outside of the torus and a negative defect in the inside of the torus, is consistent with the theoretically predicted curvature-induced unbinding for nematics on toroidal surfaces [31]. However, in the latter case the defect pair consists of ±1/2 defects. We can understand why we observe integer-strength defects from the expression for the elastic energy of a point defect in two dimensions, $E_p \propto Ls^2$, with L the Frank elastic constant [1,42]. The free energy of an integer defect is four times greater than that of a half-integer defect. However, in three dimensions, surface semi-integer defects are *always* terminal points of disclination lines which pierce the droplet's bulk, connecting two distinct surface defects. These lines contribute to the total free energy. Importantly, surface integer defects are topologically allowed to escape in the third dimension, and can therefore exist as quasi-2D features, not necessarily attached to disclination lines [43–45]. The free energy associated with a disclination line E_l is proportional to its length $\mathcal{L}$, $E_l \propto \mathcal{L}E_p$. Therefore the ratio between the free energy of a half-integer, $F_{1/2}$, and an escaped integer, F_{esc}, defect configurations, $\frac{F_{esc}}{F_{1/2}} \propto 1/\mathcal{L}$ is less than 1 for large $\mathcal{L}$, favoring the escaped integer structure [37].

To address whether the dynamics of the phase transition has an impact on the defects stability and number, we perform different sets of thermal cycles, quenching the nematic from its isotropic phase to the nematic at two different cooling rates, 2 °C/h and 2 °C/min [37]. While the nucleation and growth of the nematic phase is different for each of the two cooling rates, they both lead to configurations with an equivalent number of defect pairs, as shown in the histograms in Fig. 2(a) left, with no preferred azimuthal location, as shown in Fig. 2(a) right; the associated statistical analysis further supports these conclusions [37]. In particular, the latter observation clearly shows that the stability of the defect pairs is not due to localized imperfections in the experimental tori.

Since the theoretically predicted defect-populated state for nematics on toroidal surfaces is only expected for tori with aspect ratio below a critical value, as only then the overall energy is lowered relative to the more strained defect-free state, we generate a thinner torus, with $R \sim 810$ μm and $a \sim 101$ μm, and thus $\xi = \frac{R}{a} \approx 8$. In this case also, and irrespective of the cooling rate, we observe stable defect pairs; the probability histograms are shown in Fig. 2(b) with their associated statistical analysis in the Supplemental Material [37]. Notably, we also find stable configurations with multiple defect pairs in our computer simulations. The results are in agreement with the experiments, and support the fact that the stability of the defect pairs is not the result of local imperfections in the experimental droplets, but that, by contrast, these defective states can survive as long-lived metastable configurations of the bulk nematic, irrespectively of the Frank elastic constant L of the liquid crystal and the aspect ratio ξ of the torus.

Remarkably, we find relaxed configurations featuring ±1 defect pairs even for cylindrical nematics; see Figs. 1(c) and 1(d), for instance, and Fig. 2(c) for the probability histogram of the number of defect pairs. This clearly illustrates that the defect pairs do not arise as a result of the coupling with Gaussian curvature K, suggesting therefore a different stabilization mechanism. Once present, however, K determines the defect location, with positive defects in regions with $K > 0$ and negative defects in regions with $K < 0$. In contrast, in the cylindrical case, the location of the defect pair is degenerate; the number of defect pairs observed from the top (vertical) and the side (horizontal) is similar, and the amount of pairs that can not be visualized from either viewpoints (diagonal) is proportional to the blind spot area of the two viewing angles; this is shown in Fig. 2(d) [37].

To understand the origin of the defect pair, we use our simulations and calculate the distortion free energy of both the defect-free and defect-populated states. Our results indicate that defect annihilation of integer defects requires an

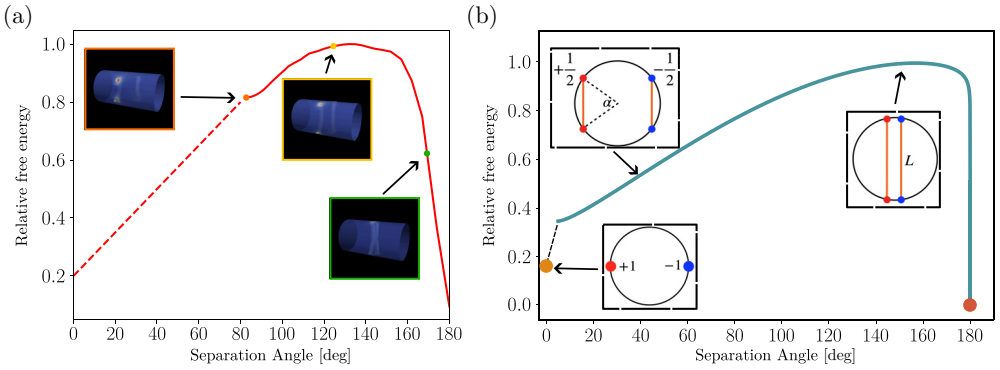

FIG. 3. (a) Relative free energy $\mathcal{F}/\max(\mathcal{F})$ for a pair of disclination lines after relaxation from the isotropic to the nematic phase. Only occasionally did this happen sufficiently far from other defects in the system for us to calculate a meaningful free energy associated with the annihilation process. The separation angle is the angle between the two half-integer defects of the same sign. The insets correspond to the configuration at the specific separation angles marked on the curve. The dash line extrapolates the elastic energy obtained from the simulation at the initial separation angle after the relaxation process to that of a pair of $s = \pm 1$ boojums at zero separation angle. (b) The same energy vs separation angle obtained from an analytical model of the same process. The insets are sketches of the configurations at different separation angles. The dash line extrapolates the results for the smallest separation angle considered in the model to the case corresponding to having a pair of $s = \pm 1$ boojums.

intermediate step in which the two integer defects split into two half-integer defects each, connected through disclination lines. Half-integer defects of opposite charge then approach each other and, eventually, annihilate, as illustrated by the insets of Fig. 3(a). Tracking the free energy evolution, we find that it first increases, as the semi-integer defects grow apart with the connecting disclination lines growing longer, to then abruptly drop once the attraction between oppositely charged defects becomes dominant. The initial separation angle of the lines is $\sim 80^{o}$, which is not far from the energy maximum to allow for the spontaneous annihilation of the disclination lines, allowing us to calculate the elastic energy. The dash line in this figure extrapolates the simulation results to what would be expected at zero sepation angle, where instead of lines we would have the ± 1 boojums. Interestingly, for micrometer-sized nematics confined to toroidal cavities with nearly square cross-sections and subjected to tangential boundary conditions, the pair of disclination lines with small separation angle is stable against the formation of the boojum pair [46], emphasizing the significance of the lines as an intermediate configuration for the system to transition to the defect-free state. Our observations ultimately suggest that the defective configurations in our experiments are separated from a defect-free state by an energy barrier, responsible for the stabilization of the ± 1 defect pairs.

We then construct an analytical model to confirm that the splitting into the two $1/2$ lines causes an energy barrier that stabilizes the defect pairs seen in experiments and simulations. We consider both free energy contributions associated to the bulk of the nematic and also surface contributions related to the defects and their interaction [37]. The initial state has two pairs of ± 1 defects that are then split into two $\pm 1/2$ defects connected by disclination lines that then approach each other to annhilate after meeting and result in the defect-free state. We indeed find that the resultant free energy profile agrees with that found in simulation, as shown in Fig. 3(b). Using values for the intervening material parameters for our nematic liquid crystal, we find that the height of barrier is $\gg k_B T$ [37],

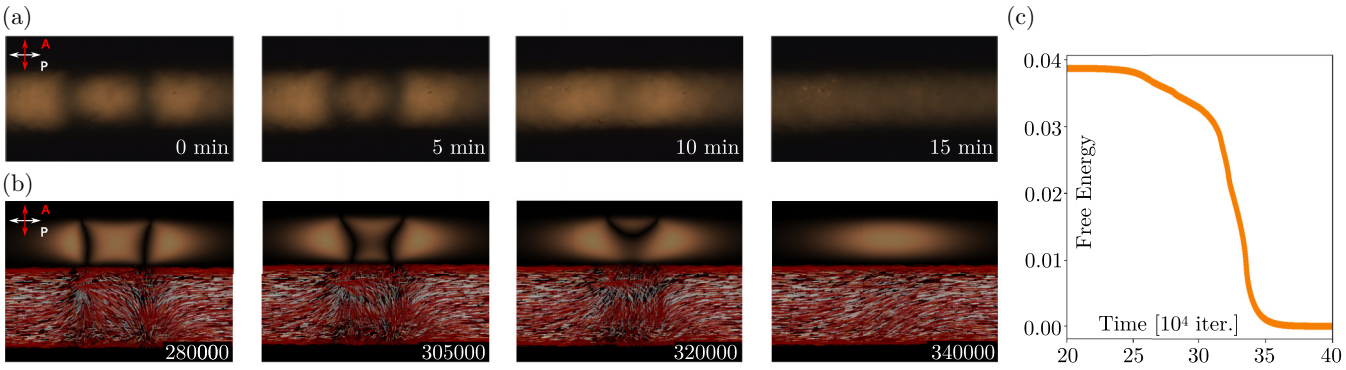

FIG. 4. (a) Annihilation of two defect pairs on a cylinder with the ± 1 defects of each pair located on opposite sides of the circular cross-section, observed through crossed polarizers in experiments. As time passes, the oppositely charged defects get closer to eventually annihilate and disappear. In the process, they leave a bright defect-free pattern that relaxes into the dark pattern observed and that corresponds to the defect-free configuration. (b) The same configuration observed in simulations. The images under crossed polarizers are shown at the top with the corresponding director field at the bottom. The iteration step of each state is noted at the bottom-right corner in each panel. (c) Free energy $(\mathcal{F} - \mathcal{F}_0)/\mathcal{F}_{\text{def}}$ vs time along the process. Note the final state is defect free and has the ground-state (zero) energy.

clearly explaining the stability of the defect-populated states. A detailed comparison between theory and simulation reveals, however, quantitative differences; this is in part due the simplicity of the model, which among other things, assumes the disclination lines are straight, while in the simulation they are clearly curved.

Irrespective of the details, defect stabilization relies on the significant energetic cost required for bulk nematic rearrangements. This is further corroborated by realizing that defect annihilation can otherwise happen if such energetic cost is avoided. Indeed, when two defect pairs in a nematic cylinder are arranged such that oppositely charged defects in each pair locate at similar polar angles, defect annihilation readily occurs both in experiments and simulations, as shown in Figs. 4(a) and 4(b). In this case, there is no energy barrier for the system to relax to its defect-free configuration, as shown in Fig. 4(c), reflecting the lack of any significant bulk rearrangement.

Our work provides experimental evidence that complex defective structures can be stabilized in bulk nematic toroidal and cylindrical droplets as long-lived metastable states. Supported by computer simulations and analytical arguments, we show that this is indeed possible because of the existence of an effective energy barrier required to rearrange the liquid crystal in the bulk into a defect-free state. Increasing the genus of the droplets will likely result in additional fascinating metastable states that are, however, yet to be studied in experiment, simulation and theory.

We thank support from MCIN/AEI/10.13039/501100011033/FEDER,UE (Grant No. PID2021-122369NB-100), the 2021 SGR 00450, the Spanish University Ministry via the FPU20/03682 grant, the Netherlands Organization for Scientific Research (NWO/OCW), as part of the Vidi scheme, the European Union via the ERC-CoGrant HexaTissue, and EMBO ALTF 353-2023. Simulations were performed on the Dutch national e-infrastructure with the support of SURF through the Grant 2021.028 for computational time. We thank Giuseppe Negro, University of Bari, for helpful discussions.

[1] P.-G. de Gennes and J. Prost, *The Physics of Liquid Crystals* (Oxford Science Publications, Oxford, UK, 1993).

[2] P. M. Chaikin and T. C. Lubensky, *Principles of Condensed Matter Physics* (Cambridge University Press, Cambridge, UK, 1995).

[3] M. Kleman and O. D. Lavrentovich, Topological point defects in nematic liquid crystals, Philos. Mag. **86**, 4117 (2006).

[4] P. J. Collings and J. W. Goodby, *Introduction to Liquid Crystals: Chemistry and Physics*, 2nd ed. (CRC Press, Boca Raton, FL, 2019).

[5] J.-C. Loudet, P. Barois, and P. Poulin, Colloidal ordering from phase separation in a liquid-crystalline continuous phase, Nature (London) **407**, 611 (2000).

[6] I. Muševič and M. Škarabot, Self-assembly of nematic colloids, Soft Matter **4**, 195 (2008).

[7] M. A. Gharbi, S. Manet, J. Lhermitte, S. Brown, J. Milette, V. Toader, M. Sutton, and L. Reven, Reversible nanoparticle cubic lattices in blue phase liquid crystals, ACS Nano **10**, 3410 (2016).

[8] A. Jangizehi, F. Schmid, P. Besenius, K. Kremer, and S. Seiffert, Defects and defect engineering in soft matter, Soft Matter **16**, 10809 (2020).

[9] H. Jeridi, J. de Dieu Niyonzima, C. Sakr, A. Missaoui, S. Shahini, A. Vlad, A. Coati, N. Goubet, S. Royer, I. Vickridge, M. Goldmann, D. Constantin, Y. Garreau, D. Babonneau, B. Croset, B. Gallas, E. Lhuillier, and E. Lacaze, Unique orientation of 1D and 2D nanoparticle assemblies confined in smectic topological defects, Soft Matter **18**, 4792 (2022).

[10] S. Das, J. Noh, W. Cao, H. Sun, N. C. Gianneschi, and N. L. Abbott, Using nanoscopic solvent defects for the spatial and temporal manipulation of single assemblies of molecules, Nano Lett. **22**, 7506 (2022).

[11] M. Cavallaro Jr., M. A. Gharbi, D. A. Beller, S. opar, Z. Shi, T. Baumgart, S. Yang, R. D. Kamien, and K. J. Stebe, Exploiting imperfections in the bulk to direct assembly of surface colloids, Proc. Natl. Acad. Sci. USA **110**, 18804 (2013).

[12] L. N. Carenza, G. Gonnella, D. Marenduzzo, G. Negro, and E. Orlandini, Cholesteric shells: Two-dimensional blue fog and finite quasicrystals, Phys. Rev. Lett. **128**, 027801 (2022).

[13] F. Vafa and L. Mahadevan, Active nematic defects and epithelial morphogenesis, Phys. Rev. Lett. **129**, 098102 (2022).

[14] Z. Wang, M. C. Marchetti, and F. Brauns, Patterning of morphogenetic anisotropy fields, Proc. Natl. Acad. Sci. USA **120**, e2220167120 (2023).

[15] L. A. Hoffmann, L. N. Carenza, J. Eckert, and L. Giomi, Theory of defect-mediated morphogenesis, Sci. Adv. **8**, eabk2712 (2022).

[16] O. D. Lavrentovich, Topological defects in dispersed words and worlds around liquid crystals, or liquid crystal drops, Liq. Cryst. **24**, 117 (1998).

[17] F. Serra, Curvature and defects in nematic liquid crystals, Liq. Cryst. **43**, 1920 (2016).

[18] T. Lopez-Leon, V. Koning, K. B. S. Devaiah, V. Vitelli, and A. Fernandez-Nieves, Frustrated nematic order in spherical geometries, Nat. Phys. **7**, 391 (2011).

[19] A. Fernandez-Nieves, D. R. Link, M. Márquez, and D. A. Weitz, Topological changes in bipolar nematic droplets under flow, Phys. Rev. Lett. **98**, 087801 (2007).

[20] U. Tkalec and I. Muevi, Topology of nematic liquid crystal colloids confined to two dimensions, Soft Matter **9**, 8140 (2013).

[21] K. He, Y. Zhou, H. Ramezani-Dakhel, J. J. de Pablo, A. Fernandez-Nieves, and T. Lopez-Leon, From nematic shells to nematic droplets: Energetics and defect transitions, Soft Matter **18**, 1395 (2022).

[22] E. Pairam, J. Vallamkondu, V. Koning, B. C. van Zuiden, P. W. Ellis, M. A. Bates, V. Vitelli, and A. Fernandez-Nieves, Stable nematic droplets with handles, Proc. Natl. Acad. Sci. USA **110**, 9295 (2013).

[23] P. W. Ellis, K. Nayani, J. P. McInerney, D. Z. Rocklin, J. O. Park, M. Srinivasarao, E. A. Matsumoto, and A. Fernandez-Nieves, Curvature-induced twist in homeotropic nematic tori, Phys. Rev. Lett. **121**, 247803 (2018).

[24] Z. S. Davidson, L. Kang, J. Jeong, T. Still, P. J. Collings, T. C. Lubensky, and A. G. Yodh, Chiral structures and defects of lyotropic chromonic liquid crystals induced by saddle-splay elasticity, Phys. Rev. E **91**, 050501(R) (2015).

[25] J. H. Erdmann, S. Zumer, and J. W. Doane, Configuration transition in a nematic liquid crystal confined to a small spherical cavity, Phys. Rev. Lett. **64**, 1907 (1990).

[26] S. Bhalla, D. T. Melnekoff, A. Aleman, V. Leshchenko, P. Restrepo, J. Keats, K. Onel, J. R. Sawyer, D. Madduri, J. Richter, S. Richard, A. Chari, H. J. Cho, J. T. Dudley, S. Jagannath, A. Lagana, and S. Parekh, Patient similarity network of newly diagnosed multiple myeloma identifies patient subgroups with distinct genetic features and clinical implications, Sci. Adv. **7**, eabg9551 (2021).

[27] P. W. Ellis, D. J. Pearce, Y.-W. Chang, G. Goldsztein, L. Giomi, and A. Fernandez-Nieves, Curvature-induced defect unbinding and dynamics in active nematic toroids, Nat. Phys. **14**, 85 (2017).

[28] T. Lopez-Leon and A. Fernandez-Nieves, Drops and shells of liquid crystal, Colloid Polym. Sci. **289**, 345 (2011).

[29] R. D. Kamien, The geometry of soft materials: a primer, Rev. Mod. Phys. **74**, 953 (2002).

[30] H. Hopf, Vektorfelder in n-dimensionalen Mannigfaltigkeiten, Math. Ann. **96**, 225 (1927).

[31] M. Bowick, D. R. Nelson, and A. Travesset, Curvature-induced defect unbinding in toroidal geometries, Phys. Rev. E **69**, 041102 (2004).

[32] V. Vitelli and A. M. Turner, Anomalous coupling between topological defects and curvature, Phys. Rev. Lett. **93**, 215301 (2004).

[33] L. Giomi and M. J. Bowick, Elastic theory of defects in toroidal crystals, Eur. Phys. J. E **27**, 275 (2008).

[34] D. Jesenek, S. Kralj, R. Rosso, and E. G. Virga, Defect unbinding on a toroidal nematic shell, Soft Matter **11**, 2434 (2015).

[35] E. Pairam and A. Fernandez-Nieves, Generation and stability of toroidal droplets in a viscous liquid, Phys. Rev. Lett. **102**, 234501 (2009).

[36] E. Pairam, H. Le, and A. Fernandez-Nieves, Stability of toroidal droplets inside yield stress materials, Phys. Rev. E **90**, 021002(R) (2014).

[37] See Supplemental Material at http://link.aps.org/supplemental/10.1103/PhysRevResearch.6.L012065 for more details on the generation of toroidal and cylindrical nematic droplets, twist angle estimation, heating and cooling of nematic droplets, statistical analysis of experimental distributions, simulation algorithm, azimuthal symmetry of defect pairs in nematic cylinders, and analytic estimation for the energy cost of disclination vs point defects.

[38] D. J. G. Pearce, P. W. Ellis, A. Fernandez-Nieves, and L. Giomi, Geometrical control of active turbulence in curved topographies, Phys. Rev. Lett. **122**, 168002 (2019).

[39] L. N. Carenza, G. Gonnella, A. Lamura, G. Negro, and A. Tiribocchi, Lattice Boltzmann methods and active fluids, Eur. Phys. J. E **42**, 81 (2019).

[40] L. N. Carenza, G. Gonnella, D. Marenduzzo, and G. Negro, Rotation and propulsion in 3D active chiral droplets, Proc. Natl. Acad. Sci. **116**, 22065 (2019).

[41] C. R. Wand and M. A. Bates, Chiral nematic liquid crystals in torus-shaped and cylindrical cavities, Phys. Rev. E **100**, 052702 (2019).

[42] S. Chandrasekhar, *Liquid Crystals* (Cambridge University Press, Cambridge, UK, 1992).

[43] C. Williams, P. Pierański, and P. E. Cladis, Nonsingular $s = +1$ screw disclination lines in nematics, Phys. Rev. Lett. **29**, 90 (1972).

[44] P. E. Cladis and M. Kléman, Nonsingular $s = +1$ screw disclination lines in nematics, J. Phys. France **33**, 591 (1972).

[45] R. B. Meyer, On the existence of even indexed disclinations in nematic liquid crystals, Philos. Mag. **27**, 405 (1973).

[46] M. G. Campbell, M. Tasinkevych, and I. I. Smalyukh, Topological polymer dispersed liquid crystals with bulk nematic defect lines pinned to handlebody surfaces, Phys. Rev. Lett. **112**, 197801 (2014).